

A theoretical comparison of energy sources—microwave, ultrasound and laser—for interstitial thermal therapy

Matthew G Skinner[†], Megumi N Iizuka[†], Michael C Kolios[‡] and Michael D Sherar[†]

[†] Ontario Cancer Institute/Princess Margaret Hospital, Medical Physics Division and Department of Medical Biophysics, University of Toronto, 610 University Avenue, Toronto, Ontario, Canada M5G 2M9

[‡] Department of Mathematics, Physics and Computer Science, Ryerson Polytechnic University, 350 Victoria Street, Toronto, Ontario, Canada M5B 2K3

Received 13 July 1998, in final form 28 September 1998

Abstract. A number of heating sources are available for minimally invasive thermal therapy of tumours. The purpose of this work was to compare, theoretically, the heating characteristics of interstitial microwave, laser and ultrasound sources in three tissue sites: breast, brain and liver. Using a numerical method, the heating patterns, temperature profiles and expected volumes of thermal damage were calculated during standard treatment times with the condition that tissue temperatures were not permitted to rise above 100 °C (to ensure tissue vaporization did not occur). Ideal spherical and cylindrical applicators (200 μm and 800 μm radii respectively) were modelled for each energy source to demonstrate the relative importance of geometry and energy attenuation in determining heating and thermal damage profiles. The theoretical model included the effects of the collapse of perfusion due to heating. Heating patterns were less dependent on the energy source when small spherical applicators were modelled than for larger cylindrical applicators due to the very rapid geometrical decrease in energy with distance for the spherical applicators. For larger cylindrical applicators, the energy source was of greater importance. In this case, the energy source with the lowest attenuation coefficient was predicted to produce the largest volume of thermally coagulated tissue, in each tissue site.

1. Introduction

Minimally invasive thermal therapy is an experimental cancer treatment used to destroy solid tumours in a variety of sites. In contrast to traditional hyperthermia, where tissue temperatures are elevated to the 40–45 °C range and which is used as an adjuvant to conventional therapies, thermal therapy employs much higher temperatures (50 °C to 90 °C) over shorter times (seconds to minutes), and can be used as a stand-alone therapy.

Interstitial heating is currently the most commonly used method of heating tumours because energy can be localized to the target volume while surrounding healthy tissue is preserved. A number of different energy sources are used to deliver thermal energy including laser light, microwaves and ultrasound. Interstitial photocoagulation has been used to treat liver metastases (Amin *et al* 1993), primary liver tumours (Vogl *et al* 1995) and breast cancer (Mumtaz *et al* 1996). Interstitial microwave thermal therapy has been used to treat primary liver hepatocellular carcinomas (Hamazoe *et al* 1995).

In parallel with these investigations, clinical studies using a combination of medical imaging (MRI or ultrasound) and interstitial thermal therapy are under way to determine if

tissue temperatures and the development of thermal damage can be monitored in real time. These studies, conducted in several sites including the brain (Schrottner *et al* 1990), liver (Hahl *et al* 1990, Dowlatahi *et al* 1992) and the breast (Steger *et al* 1989), are critical to the widespread implementation of thermal therapy techniques because of the possibility of producing controlled thermal coagulation without destroying surrounding normal tissue.

Given the choice of heating modalities currently available, the question arises as to which is the optimum energy source for a particular tumour site. Few studies have compared the ability of different heating modalities to deliver energy for thermal therapy. Comparative studies have been conducted in the past in the hyperthermia temperature range, 40–45 °C (Greguss 1991), but these have mainly focused on the mechanisms causing cell death, rather than evaluating the relative effectiveness of the various modalities in depositing power in tissue.

To address this problem we employed a theoretical approach to compare power deposition, temperature distributions and thermal damage profiles for two applicator geometries (spherical and cylindrical) in three different tissue sites (breast, brain and liver) using three energy sources (810 nm laser light, 1 GHz microwaves and 1 MHz ultrasound). Although the applicators modelled are not realized practically, the model gives insight as to the relative importance of energy fall-off due to geometry, attenuation of the energy in tissue, and blood flow. The tissue sites were chosen based on the potential clinical application of thermal therapy. Tumours located in the brain or the liver are often unresectable due to their proximity to critical normal tissues, making minimally invasive thermal therapy a potential alternative. Tumours in the breast are normally candidates for surgery. However, if minimally invasive procedures such as thermal therapy can demonstrate equal effectiveness in destroying tumour tissue, an advantage may be gained due to the expected preservation of normal tissue architecture.

2. Materials and methods

2.1. Theory

The theoretical modelling was broken down into three steps:

(i) The specific absorption rate (SAR; W cm^{-3}) was calculated using known attenuation properties of each tissue for the different energy sources. The SAR was calculated for both a spherical source and a cylindrical source of infinite length (see figure 1) for each of the three energy sources.

(ii) The temperature distribution was calculated as a function of time using the SAR as an input to the Pennes bioheat transfer equation (Pennes 1948).

(iii) Thermal damage was calculated as a function of time using the temperature history as input for an Arrhenius model of cell kill (Henriques 1947).

For laser light, absorption was modelled using the light diffusion approximation for monoenergetic neutral particles which is an approximate solution to the radiative transport equation (Weinberg and Wigner 1958). The diffusion approximation is valid when the scattering coefficient is much larger than the absorption coefficient ($\mu_s \gg \mu_a$), which is the case in most soft tissues (Cheong *et al* 1990). The SAR for a spherical laser source is given by (Welch and van Gemert 1995)

$$\text{SAR} \propto \frac{P_0 R_0 \exp[-\mu_{\text{eff}}(R - R_0)]}{R} \quad (R > R_0) \quad (1)$$

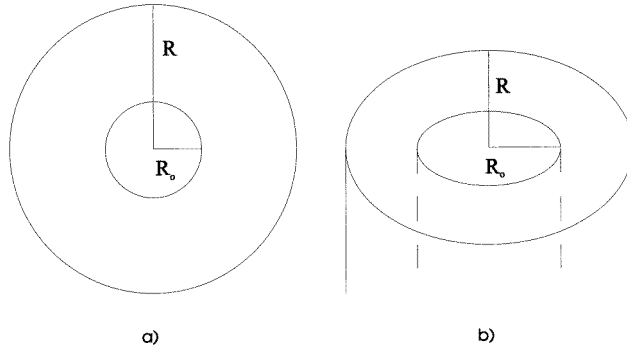


Figure 1. Schematic diagram of the two applicator geometries that were simulated: (a) a spherical applicator with radius $R_0 = 200 \mu\text{m}$; (b) an infinite cylinder with radius $R_0 = 800 \mu\text{m}$. The computational domain was 20 cm in radius for both cases.

where R (cm) is the radial distance from the centre of the applicator, R_0 (cm) is the radius of the spherical applicator, P_0 (W cm^{-3}) is the power radiating from the applicator source and μ_{eff} (cm^{-1}) is the effective attenuation coefficient of the tissue being modelled. The effective attenuation coefficient for light is given by (Welch and van Gemert 1995)

$$\mu_{\text{eff}} = [3\mu_a(\mu_a + \mu'_s)]^{1/2} \quad (2)$$

where μ'_s (cm^{-1}), the reduced scattering coefficient, is equal to $\mu_s(1 - g)$ where g is the anisotropy coefficient. the SAR for an infinitely long cylindrical laser source is given by (Welch and van Gemert 1995)

$$\text{SAR} \propto \frac{P_0 R_0^{1/2} \exp[-\mu_{\text{eff}}(R - R_0)]}{R^{1/2}} \quad (R > R_0) \quad (3)$$

where R_0 is now the radius of the cylindrical applicator.

The SAR expressions for ultrasound and microwave sources are based on the propagation of mechanical and electromagnetic waves. For both ultrasound and microwave spherical sources, the SAR is given by (King and Smith 1981)

$$\text{SAR} \propto \frac{P_0 R_0^2 \exp[-2\mu(R - R_0)]}{R^2} \quad (R > R_0) \quad (4)$$

where μ is the attenuation coefficient of the ultrasound or microwaves in the tissue. For an infinite cylinder the ultrasound or microwave SAR applicator is (King and Smith 1981)

$$\text{SAR} \propto \frac{P_0 R_0 \exp[-2\mu(R - R_0)]}{R} \quad (R > R_0). \quad (5)$$

In contrast to ultrasound and microwave spherical sources where $\text{SAR} \propto 1/R^2$, the spherical laser source has an $\text{SAR} \propto 1/R$. The $1/R$ relationship for light is a result of multiple scattering which results in a contribution to the fluence and SAR of light that has been scattered back into the line of propagation. The differences in equations for the cylindrical sources are explained by the same phenomenon.

Simulations were conducted for a $200 \mu\text{m}$ radius spherical source and an $800 \mu\text{m}$ radius cylindrical source. These radii were chosen to demonstrate the relative importance of geometry and tissue properties in determining the kinetics of heating. The $200 \mu\text{m}$ radius spherical source was expected to have a very rapid geometrical fall-off in energy, such that the effect of tissue attenuation may be less important. The $800 \mu\text{m}$ radius cylindrical

applicators were expected to have a less rapid fall off with increasing radial distance due to geometry. Therefore the tissue attenuation properties were expected to have greater importance in determining the SAR patterns of these applicators.

The simulations modelled the use of 1 MHz ultrasound, 1 GHz microwaves and 810 nm laser light. These frequencies and wavelengths are typical of those used in thermal therapy. The SAR was calculated for the two geometries in each of the three tissues chosen: breast, brain (white matter) and liver. The physical parameters used for each tissue are shown in table 1.

Table 1. Tissue parameters used in simulating power deposition for ultrasound, microwave and laser in breast, brain and liver.

Properties	Breast	Brain	Liver
k (W cm ⁻¹ K ⁻¹)	0.004 99 ²	0.005 03 ¹	0.005 28 ³
c (J g ⁻¹ K ⁻¹)	3.55 ⁴	3.60 ¹	3.60 ¹
ρ (g cm ⁻³)	1.02*	1.043*	1.050*
w_b (g cm ⁻³ s ⁻¹)	0.000 699 ⁶	0.010 29 ⁵	0.018 73 ⁵
$1/\mu$ (cm)			
ultrasound	4.54 ⁸	11.11 ⁷	29.4 ⁹
microwave	5.51 ¹¹	1.37 ¹⁰	3.83 ¹²
laser ($1/\mu_{\text{eff}}$)	0.46 ¹⁴	0.233 ¹³	0.27 ¹⁵

* ICRP (1975), ICRU (1989), Woodward and White (1986), Diem and Lentner (1970).

¹ Cooper and Trezek (1972).

² Bowman (1981).

³ Valvano *et al* (1985).

⁵ Williams and Leggett (1989).

⁶ Beaney *et al* (1984).

⁷ Bamber and Hill (1981).

⁸ Goss *et al* (1978).

⁹ Lyons and Parker (1988).

¹⁰ Foster *et al* (1979).

¹¹ Burdette (1982).

¹² Schwan and Li (1953).

¹³ Roggan *et al* (1995).

¹⁴ Ertefai and Profio (1985).

¹⁵ Welch and van Gemert (1995).

The SAR (Q) was used as an input into the Pennes bioheat transfer equation (BHTE) (Pennes 1948) which models heat transfer in tissue, to calculate temperature T as a function of time t and distance R from the source in the tissue:

$$\rho c \partial T / \partial t = k \nabla^2 T - c_b w_b (T - T_a) + Q \quad (6)$$

where ρ is the density of the tissue (g cm⁻³), c is the specific heat capacity (J g⁻¹ K⁻¹), k is the thermal conductivity (W cm⁻¹ K⁻¹) and w_b is the blood perfusion (g cm⁻³ s⁻¹). $k \nabla^2 T$ represents heat conduction, while $c_b w_b (T - T_a)$ is a heat sink term representing the removal of heat by blood in the microvasculature. The perfusion term w_b in equation (6) was not a constant but varied to account for collapse of the microvasculature perfusion during heating. The value of w_b at any location and time was calculated from an Arrhenius damage integral:

$$\Omega(r, t) = \int_{t=0}^{t=t} A_{\text{freq}} \exp[-E_a / (RT(t))] dt \quad (7)$$

where E_a and A_{freq} , the activation energy and frequency factor respectively, were calculated from changes in blood flow due to heating measured by Brown *et al* (1992). Those data lead to an E_a and A_{freq} for blood flow collapse of 6.67×10^5 (J mol⁻¹) and 1.98×10^6 (s⁻¹) respectively. w_b was then calculated continuously during the treatment as

$$w_b(r, t) = w_{\text{init}}(1 - e^{-\Omega}) \quad (8)$$

where w_{init} is the baseline blood flow (taken from table 1) before treatment begins.

The presence of a temperature-dependent term w_b in the Pennes bioheat equation required a modified finite difference approach to solve the nonlinear form of the equation (Croft and Lilley 1990). The temperature was first calculated assuming initial (for the first time step) or previous (for all later time steps) values of the blood perfusion. This initial temperature calculation was used to calculate a new value for blood perfusion. The temperature was recalculated assuming the new blood flow value and compared with the initial temperature calculation. If the difference between the two temperatures was within a tolerance set at 0.1% of the initial calculated value, the updated temperature was stored as the result for the time step. If the difference was larger than the tolerance, the temperature was recalculated using the new blood flow values based on the second temperature calculation. The process was repeated at each time step until the change in temperature was less than 0.1% of the previous temperature calculation. The numerical model utilized a radial step size $dr = 0.01$ cm and a temporal step size $dt = 0.037$ s for all simulations.

Temperature profiles as a function of time at each location were used to calculate tissue damage. This calculation, as with the blood flow damage, was also based on an Arrhenius damage integral (equation (7)) where now $e^{-\Omega} = c(t)/c(0)$, $c(t)$ is the concentration of native undamaged cells at time t , $c(0)$ is the initial concentration at time $t = 0$. E_a (5.06×10^5 J mol⁻¹) and A_{freq} (2.98×10^8 s⁻¹) were determined from families of cell survival curves for BHK (baby hamster kidney) cells exposed to elevated temperatures up to a maximum of 57 °C as a function of time (Borrelli *et al* 1990). E_a and A_{freq} are the slope and intercept respectively of a plot of $\ln(1/D_0)$ versus $1/T$, where D_0 is the slope of the exponential portion of the cell survival curves. It was assumed, in the absence of available data at higher temperatures, that this Arrhenius relationship is valid over the entire temperature range that was studied, 37 °C to 97 °C. This assumption is not accurate in the 37 °C to 43 °C range, due to a 'break point' in the Arrhenius curve, normally seen at approximately 43 °C (Hall 1994). This was not expected to have a significant effect on the calculated thermal damage profile due to the very low expected damage below this 'break point' for the short treatments modelled here.

The SAR was scaled in these calculations such that the BHTE would produce a final temperature of 60 °C above ambient (equivalent to 97 °C at the applicator edge). This temperature was chosen so that the simulated therapy avoided tissue vaporization. This is an important consideration because vaporization can lead to unpredictable volumes of thermal damage due to rapidly changing tissue properties.

3. Results

Figure 2 shows the calculated SAR profiles in breast (*a, b*) brain (white matter) (*c, d*) and liver (*e, f*) for the spherical and cylindrical sources respectively in each tissue. Several features of these plots are of interest. First, the decline of SAR with distance is much more rapid for the spherical source than for the cylindrical source for all energy sources and tissue types. This is quantified in table 2 which gives the distances at which the SAR falls to 30% of its level at the applicator surface (unity in the normalized plots of figure 2). These

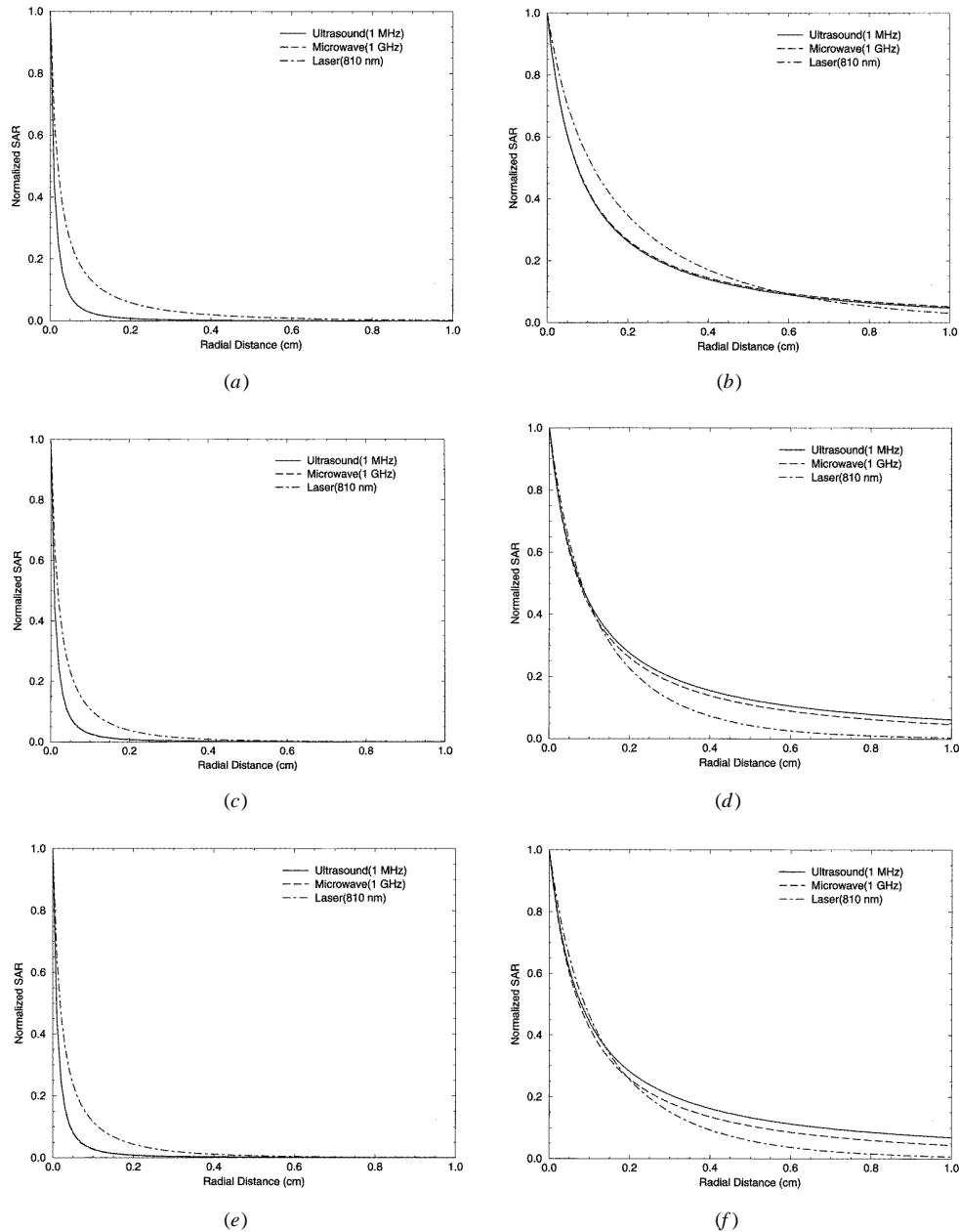


Figure 2. Normalized SAR profiles as a function of radial distance generated by the theoretical model. Figures (a), (c) and (e) are for the spherical applicator with a radius of 200 μm in breast, brain and liver respectively. Figures (b), (d) and (f) are infinite cylindrical applicators with an applicator radius of 800 μm in breast, brain and liver.

distances are relatively independent of tissue type even though the attenuation characteristics of the tissues are quite different, particularly for 810 nm laser light. As expected, the laser SAR falls off less rapidly with distance than for either microwaves or ultrasound. This is

Table 2. Distance from the applicator surface (in mm) where the SAR is 30% of its maximum value for both spherical and cylindrical geometry in breast, brain (white matter) and liver tissue.

Geometry	Modality	Breast	Brain	Liver
Spherical	Ultrasound	0.18	0.18	0.18
	Microwave	0.18	0.18	0.18
	Laser	0.41	0.38	0.38
Cylindrical	Ultrasound	1.7	1.8	1.8
	Microwave	1.7	1.7	1.6
	Laser	2.2	1.5	1.7

due to the $1/R$ factor in the laser SAR compared to the $1/R^2$ factor for ultrasound and microwaves.

In the case of the cylindrical source which is both larger in diameter and more distributed (it is an infinite line source), the attenuation properties play a more important role in determining the SAR profile for the tissues studies. This is observed in figure 2 where the SAR profiles vary to a much greater degree for the spherical source. However, the 30% SAR distance is still similar for all energy sources in liver and brain and slightly greater for the laser source in breast tissue. The cylindrical source SAR profiles illustrate the competing roles of tissue attenuation properties and the geometrical factor in determining the SAR. The laser SAR falls off least rapidly close to the applicator where the geometry factor is most important, whereas it falls off most rapidly further from the applicator where the tissue attenuation factor in the SAR equation becomes more important. This transition occurs furthest from the applicator in breast tissue in which laser light attenuation is lowest. The differences in attenuation between ultrasound and microwaves also result in larger differences in SAR profiles for the cylindrical sources as compared with the spherical sources.

Figure 3 shows the temperature profiles calculated when the SAR values for the cylindrical source in figure 2 were used as an input to the BHTE equation including the effects of changing blood flow during heating. The temperature profiles were calculated at the end of 1 min (*a, b*) and 10 min treatment times (*c, d*) in breast and liver respectively in each case. The temperature profiles for the 1 min treatments are similar in shape to the SAR profiles because conduction and blood perfusion have had little time to affect the increase in temperature. However, for 10 min treatments, the temperature profiles become more dependent on conduction and perfusion. The ultrasound source produces more deeply penetrating high temperatures than does the laser. This is primarily due the greater importance of energy deposition far from the applicator for longer treatment times. Ultrasound achieves the greatest penetration for the cylindrical applicator (figures 2(*b*) and 2(*f*)). Also of note is the observation that the laser produces a narrower temperature distribution in liver than in breast because of the larger absorption of light in liver than in breast.

Progression of the thermal damage boundary during the 10 min treatments including a 10 min cooling period (heating power turned off) are shown in figure 4 for (*a*) breast and (*b*) liver. The lesion created in breast is larger than for liver for all energy sources due to the lower perfusion in breast. The lower perfusion also results in the lesion continuing to grow in breast after the power has been switched off, whereas the lesion remains constant in size after the power is switched off in liver. Ultrasound produced the largest thermal

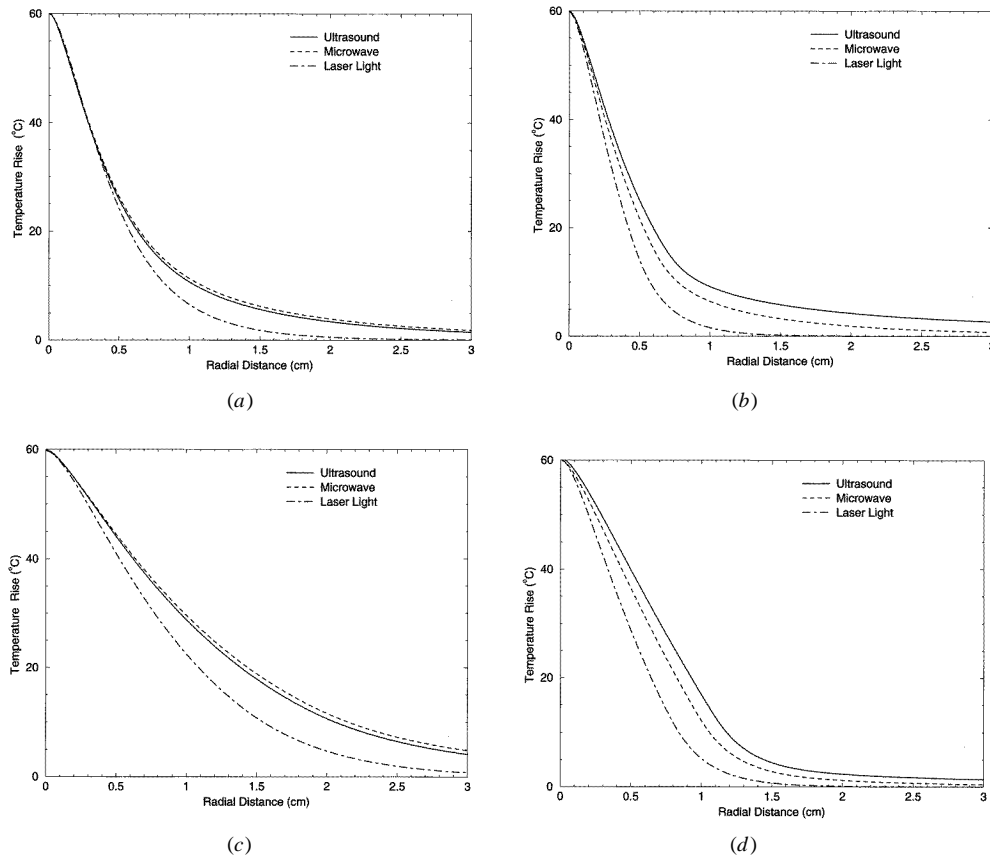


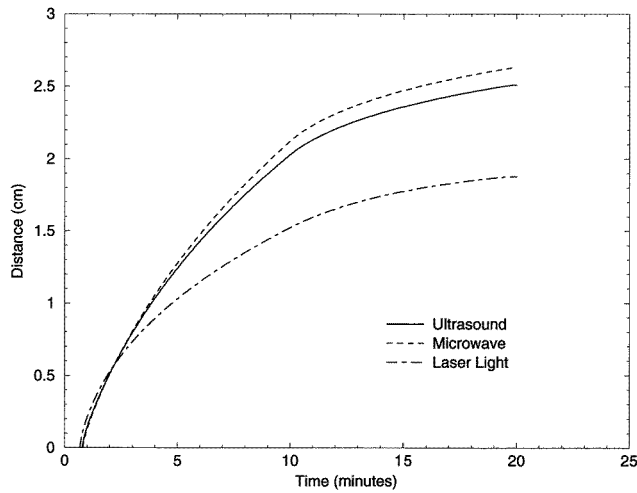
Figure 3. Temperature versus radial distance profiles. All profiles assumed an infinite cylindrical geometry and the temperature rise is with respect to 37°C. Figures (a) and (c) were simulated in breast tissue for 1 min and 10 min respectively. Figures (b) and (d) were simulated in liver tissue for 1 min and 10 min respectively.

Table 3. Predicted thermal lesion radius in mm ($\Omega = 1$, equivalent to 36.8% cell survival) for an 800 μm radius infinite cylindrical applicator and a 10 min treatment time followed by a 10 min cooling period.

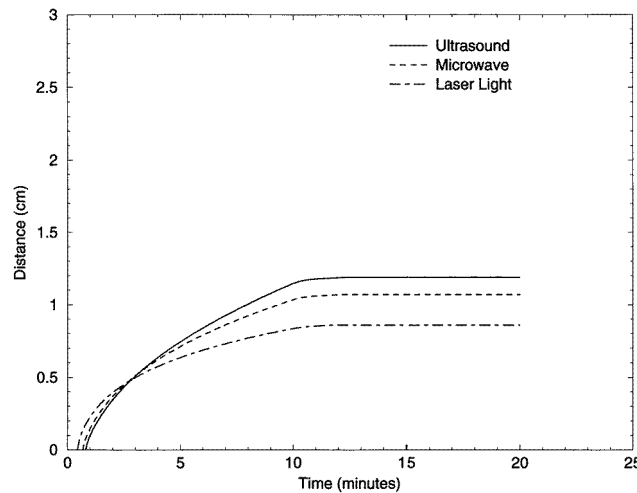
	Breast	Brain (white matter)	Liver
Ultrasound (1 MHz)	25.1	14.3	11.9
Microwave (1 GHz)	26.3	13.1	10.7
Laser (810 nm)	18.8	9.5	8.6

lesion in liver while microwaves produced the largest lesion in breast. The laser source produced a significantly smaller lesion in both tissues. Table 3 shows the radial extent of thermal damage ($\Omega = 1$, equivalent to 36.8% cell survival) for breast, brain and liver after the 10 min treatment and 10 min cooling periods.

The importance of including the effects of changing blood flow during treatment due to vascular collapse is illustrated in figure 5. If constant flow is assumed and the same



(a)



(b)

Figure 4. Progression of thermal damage boundary for the 10 min treatments in (a) breast and (b) liver including a 10 min cooling period. Infinite cylindrical geometry sources were simulated.

power applied to the applicator as in the dynamic flow case, a much lower temperature increase is achieved during treatment. If the power is adjusted in the model to achieve the same applicator surface temperature at the end of treatment then a temperature profile with a different shape is predicted (single dashed curve in figure 5(a)). The thermal damage calculation for these different models also produced different results. If constant flow is assumed, a much smaller lesion is predicted than for dynamic flow conditions, at the same power. If the power is adjusted to give the same final applicator surface temperature (this requires a more than three-fold greater power for the dynamic blood flow case) a larger lesion is predicted when constant flow is modelled.

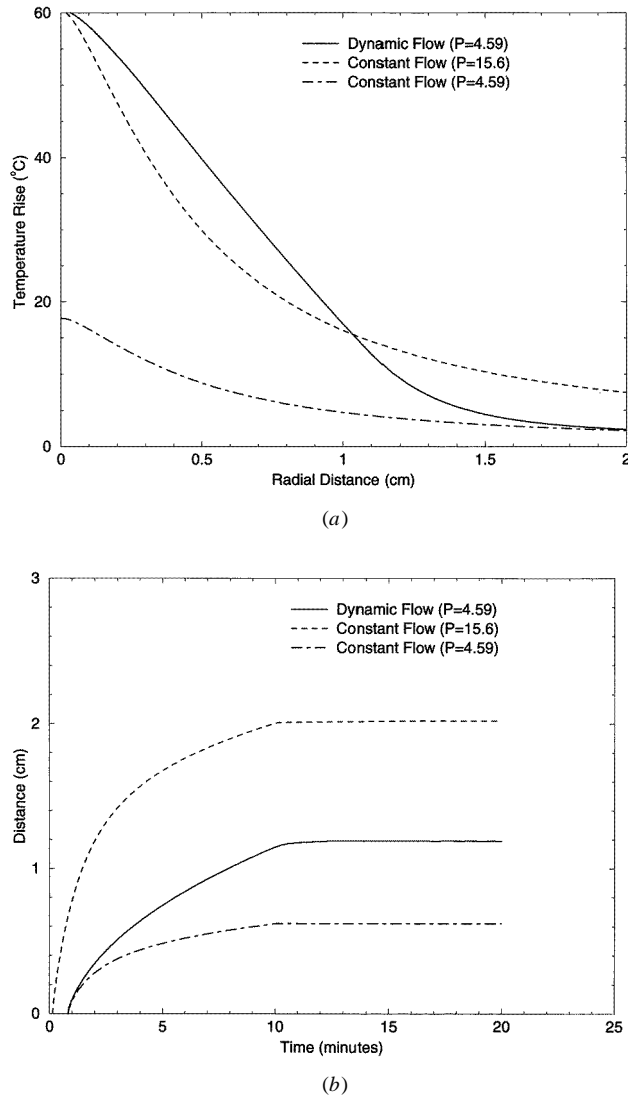


Figure 5. Effect of different blood perfusion models on temperature and cell damage. In (a) dynamic blood flow requires one-third the input power required when using constant blood flow to achieve the same final temperature of 60°C above ambient (37°C). (b) The resultant damage when the dynamic and constant flow are used. With constant blood flow set to the same input power as the dynamic perfusion, the thermal lesion produced is only one-third the radius of that produced with dynamic blood flow.

4. Discussion

We have taken a simplified approach to comparing microwaves, ultrasound and laser light as sources for thermal therapy in different tissue sites. Specifically, we have assumed that the sources have idealized spherical or cylindrical geometries. The purpose of the paper was to illustrate the competing effects of different tissue energy attenuation coefficients, applicator geometry and blood flow on thermal therapy. We decided to restrict geometry

to the idealized cases to achieve this goal. The results suggest that the choice of energy source for interstitial thermal therapy depends on a number of variables including tissue attenuation properties which depend on the target site, applicator geometry and perfusion. In general, the decrease of energy with distance due to geometry is more important close to the applicator while the fall-off due to attenuation becomes more important further from the applicator. Consequently, laser light, which is highly scattered in tissue, falls off less rapidly close to the applicator than either ultrasound or microwaves. However, further from the applicator the light fluence falls off more rapidly than ultrasound or microwaves because of the higher attenuation of laser light.

When the SAR profiles were used to calculate temperatures and thermal damage, the perfusion was observed to be the most important variable in determining the depth of heating and thermal damage. Also, for low-perfusion tissues such as breast, the thermal lesion radius can increase by as much as 15% (equivalent to a 50% increase in volume) after the power is switched off, while for high-perfusion tissues such as liver, the thermal damage volume is not expected to increase after the power is switched off. For each particular tissue, the energy source with the lowest attenuation coefficient produced the largest volume of thermal damage: microwaves in breast and ultrasound in liver.

The importance of including the effects of changing blood flow due to thermal damage is illustrated in figure 5. The power required to achieve the target temperature is lower and the volume of thermal damage predicted is higher if the collapse of perfusion is modelled. More sophisticated models that include the increase in flow due to moderate increases in temperature followed by the vascular collapse that occurs at higher temperatures will be important future developments.

The calculations presented include another important assumption; the attenuation and absorption properties of the tissue are assumed to be constant throughout the treatment. We recently reported that the ultrasound attenuation in liver, for example, increases significantly as a function of increasing temperature and time (Gertner *et al* 1997). Light absorption and scattering properties of tissues also change as tissue coagulates (Nau *et al* 1997). The inclusion of attenuation coefficients that change with accumulated thermal damage is expected to change the predicted damage radii. This is particularly important for laser light where tissue scattering coefficients can change by factors of four or more when coagulation occurs. Inclusion of all significant variables into a more sophisticated nonlinear model will be more important for planning patient treatments.

Acknowledgments

The authors would like to thank Ms Anna Sergiou for preparing the manuscript. This work was supported with a grant from the National Cancer Institute of Canada with funds from the Terry Fox Run and the Canadian Cancer Society. MNI was supported by the Jack Cunningham Fellowship at the OCI.

References

- Amin Z, Donald J J, Master A, Kant R, Steger A C, Bown S G and Lees W R 1993 Hepatic metastases: interstitial laser photocoagulation with real-time US monitoring and dynamic CT evaluation of treatment *Radiology* **187** 339-47
- Bamber J C and Hill C R 1981 Acoustic properties of normal and cancerous human liver-I Dependence on pathological condition *Ultrasound Med. Biol.* **7** 121-33

- Beaney R P, Lammertsma A A, Jones T, McKenzie C G and Halnan K E 1984 Positron emission tomography for *in vivo* measurement of regional blood flow, oxygen utilization and blood volume in patients with breast carcinoma *Lancet* **1** 131–4
- Borrelli M J, Thompson L L, Cain C A and Dewey W C 1990 Time-temperature analysis of cell killing of BHK cells heated at temperatures in the range of 43.5 °C to 57.0 °C *Int. J. Radiat. Oncol. Biol. Phys.* **19** 289–99
- Bowman H F 1981 Heat transfer and thermal dosimetry *J. Microwave Power* **16** 121–33
- Brown S L, Hunt J W and Hill R P 1992 Differential thermal sensitivity of tumour and normal microvascular response during hyperthermia *Int. J. Hyperth.* **8** 501–14
- Burdette E C 1982 Electromagnetic and acoustic properties of tissues *Physical Aspects of Hyperthermia (AAPM Medical Physics Monographs 8)* ed G H Nussbaum (New York: AIP) pp 105–50
- Cheong W F, Prahl S A and Welch A J 1990 A review of the optical properties of biological tissues *IEEE J. Quantum Electron.* **26** 2166
- Cooper T E and Tezek G J 1972 A probe technique for determining the thermal conductivity of tissue *J. Heat Transfer. Trans. ASME* **94** 133–40
- Croft D R and Lilley D G 1990 *Heat Transfer Calculations Using Finite Difference Equations* (London: Applied Science Publishers)
- Diem K and Lenter C (eds) 1970 *Documenta Geigy Scientific Tables* 7th edn (Macclesfield: Geigy)
- Dowlatahi K, Bhattacharya A K, Silver B, Matalon T and Williams J W 1992 Percutaneous interstitial laser therapy of a patient with recurrent hepatoma in a transplanted liver *Surgery* **112** 603–6
- Ertefai S and Profio A E 1985 Spectral transmittance and contrast in breast diaphanography *Med. Phys.* **12** 393–400
- Foster K R, Schepps J L, Stoy R D and Schwan H P 1979 Dielectric properties of brain tissue between 0.01 and 10 GHz *Phys. Med. Biol.* **24** 1177–87
- Gertner M R, Wilson B C and Sherar M D 1997 Ultrasound properties of liver tissue during heating *Ultrasound Med. Biol.* **23** 1395–403
- Goss S A, Johnston R L and Dunn F 1978 Comprehensive compilation of empirical ultrasonic properties of mammalian tissue *J. Acoust. Soc. Am.* **24** 423–57
- Greguss P 1991 Comparative studies on hyperthermia induced by laser light, microwaves and ultrasonics *Proc. SPIE* **1525** 313–24
- Hahl J, Haapiainen R and Orsaka J 1990 Laser-induced hyperthermia in the treatment of liver tumours *Lasers Surg. Med.* **10** 319–21
- Hall E J 1994 *Radiobiology for the Radiologist* (Philadelphia, PA: Lippencott)
- Hamazoe R, Hirooka Y, Ohtani S, Katoe T and Kabara N 1995 Intraoperative microwave tissue coagulation as treatment for patients with nonresectable hepatocellular carcinoma *Cancer* **75** 794–800
- Henriques F C 1947 The predictability and significance of thermally induced rate processes leading to irreversible epidermal injury *Arch. Pathol.* **43** 489–502
- ICRP 1975 Report of the task group on reference man *ICRP Publication 23* (Oxford: Pergamon)
- ICRU 1989 Tissue substitutes in radiation dosimetry and measurement *ICRU Report 44* (Bethesda, MD: International Commission of Radiation Units and Measurements)
- King R W and Smith G S 1981 *Antennas in Matter—Fundamental, Theory and Applications* (Cambridge, MA: MIT Press)
- Lyons M E and Parker K J 1988 Absorption and attenuation in soft tissues II—Experimental results *IEEE Trans. Ultrason. Ferroelectr. Freq. Control* **35** 511–21
- Mumtaz H, Hall-Craggs M A, Wotherspoon A, Paley M, Buonaccorsi G, Amin Z, Wilkinson I, Kissin M W, Davidson T I, Taylor I and Brown S G 1996 Laser therapy for breast cancer: MR imaging and histopathologic correlation *Radiology* **200** 651–8
- Nau W H, Roselli R J and Milam D F 1997 Effect of thermal changes on optical properties in fresh and previously frozen prostate tissue *Proc. SPIE* **2970** 476–83
- Pennes H H 1948 Analysis of tissue and arterial blood temperatures in the resting human forearm *J. Appl. Physiol.* **1** 93–122
- Roggan A, Dorschel K, Minet O, Wolff D and Muller G 1995 The optical properties of biological tissue in the near infrared wavelength range—review and measurements *Laser-induced Interstitial Thermo-therapy* ed G Muller and A Roggan (Washington, DC: SPIE Optical Engineering Press)
- Schrottner O, Ascher P W and Ebner F 1990 Interstitial laser thermo-therapy of brain tumour under MRI control *Fifth Int. Congress of the European Laser Association* p 66
- Schwan H P and Li K 1953 Capacity and conductivity of body tissues at ultra high frequencies *Proc. IRE* **41** 1735–40
- Steger A C, Lees W, Walmsley K and Brown S G 1989 Interstitial laser hyperthermia: a new approach to local destruction of tumours *Br. Med. J.* **299** 362–5

- Valvano J W, Cochran J R and Diller K R 1985 Thermal conductivity and diffusivity of biomaterials measured with self-heating thermistors *Int. J. Thermophys.* **6** 301–11
- Vogl T J *et al* 1995 Malignant liver tumours treated with MR imaging-guided laser-induced thermotherapy: technique and prospective results *Radiology* **196** 257–65
- Weinberg A M and Wigner E P 1958 *The Physical Theory of Neutron Chain Reactors* (Chicago, IL: University of Chicago Press)
- Welch A J and van Gemert M J C 1995 *Optical-Thermal Response of Laser-Irradiated Tissue* (New York: Plenum)
- Williams L R and Leggett R W 1989 Reference values for resting blood flow to organs of man *Clin. Phys. Physiol. Meas.* **10** 187–217
- Woodward H Q and White D R 1986 The composition of body tissues *Br. J. Radiol.* **59** 1209–19